Effect of random anisotropy on magnetization reversal in dipolarly coupled layered thin films

N. Chowdhury[1], S. Bedanta[1*], G. S. Babu[1], A. Weber[2], S. Mattauch[2], Ashutosh Rath[3], M. K. Dalai[4,5,6] and Thomas Brückel[7]

1.Laboratory for Nanomagnetism and Magnetic Materials (LNMM), School of Physical Sciences, National Institute of Science Education and Research (NISER), HBNI, Jatni-752050, India

2.Jülich Centre for Neutron Science (JCNS), Heinz Maier-Leibnitz Zentrum (MLZ), Forschungszentrum Jülich GmbH, Lichtenbergstr. 1, 85748 Garching, Germany

3.Institute of Physics, Bhubaneswar- 751005, India

4.CSIR – Institute of Minerals and Materials Technology, Bhubaneswar – 751013, Odisha, India

5.Academy of Scientific and Innovative Research (AcSIR), Ghaziabad – 201002, India

6.CSIR – National Physical Laboratory, Dr. K. S. Krishnan Marg, New Delhi– 110012, India

7.PGI-4: Scattering Methods Forschungszentrum Jülich GmbH 52425 Jülich, Germany

---

Abstract

Magnetic thin films and multilayers offer many novel physical phenomena with tremendous potential for applications. Various growth processes and methods are in place to make homogeneous films. However, dispersion in local easy axes is an inherent issue which may give rise to an effective random anisotropy in thin film. It is important to investigate the effect of random anisotropy on the magnetic properties of the thin films. In this report we address the aspect of local dispersion induced random anisotropy on magnetization reversal in ferromagnetic (FM)/non-magnetic(NM)/ferromagnetic(FM) stacks. We show that the magnetization reversal is not only governed by the inter-layer interaction but the intrinsic anisotropies also play a crucial role. In this context we have studied the magnetization reversal of Co/AlO_X/Co trilayers with various thicknesses of AlO_X which acts as a spacer between the two Co layers. Presence of random anisotropy in addition to growth induced uniaxial anisotropy was observed in all the samples. Magneto-optic

Kerr effect (MOKE) based microscopy revealed dipolar-coupled layer-by-layer magnetization reversal of the Co layers which was corroborated by polarized neutron reflectometry (PNR) experiments. Micromagnetic simulations confirmed that the presence of random anisotropy in addition to uniaxial anisotropy leads to layer-by-layer magnetization reversal.

Keywords: Magnetic anisotropy, Magnetic domains, Magnetization reversal

---

1. Introduction:

Ferromagnetic (FM) multilayers separated by non-magnetic (NM) spacers have been extensively studied for the advancement of fundamental research as well as data storage technology [1, 2].Whether the NM spacer is metallic or insulating one can observe novel magnetic phenomena such as giant magnetoresistance (GMR)[3] and tunnelling magnetoresistance (TMR)[4], respectively. These systems are used in magnetic sensors, read head of hard disks, and magnetic random access memory (MRAM) etc. Such applications demand the presence of uniaxial anisotropy with high saturation field and low coercivity. These properties in FM/NM/FM trilayers can be tuned for their use in applications by understanding their magnetization reversal processes. In recent years inter-layer interactions is again getting attention in the topic of skyrmions and synthetic antiferromagnets.[5, 6] The intrinsic anisotropy plays a crucial role in determining the ground state of the system. The energy density of a ferromagnetic material with uniaxial anisotropy (K_u) in the presence of external magnetic field H, is given by:

$$E = A(\vec{\bigtriangledown}\phi)^2 + K_u sin^2\phi - \mu_0\vec{H}\cdot\vec{M} - \frac{1}{2}\mu_0\vec{H}_{stray}\cdot\vec{M} \tag{1}$$

where, A is the exchange constant, ϕ is the angle between the easy axis (EA) and the magnetization $\vec{M}$ of the ferromagnetic material, μ_0 is the permeability of free space and $\vec{H}_{stray}$ is the stray field.

However, irrespective of the thin film growth techniques, a distribution of local granular anisotropy and stress may be present in thin films. This misalignment of local grain anisotropy leads to so-called random anisotropy which may affect the magnetization reversal of thin films. [7, 8] These variations in microstructures may lead to interesting behaviours such as random-anisotropy scaling [9], remanence enhancement [10], micromagnetic localization [11], collapse of hard axis [8] etc. If the EA of the grains are

completely random such that $\ll n(r) \gg = 0$, then it leads to isotropic behaviour of the thin film. However, partially misaligned EA of grains are found in polycrystalline [12] and in strained amorphous magnets [13] giving rise to the presence of a non-negligible random anisotropy in the film. Random anisotropy models were presented by Alben and Herzer [14, 15] where an effective anisotropy was observed due to the statistical averaging of the magneto-crystalline anisotropy of grains. By introducing random anisotropy, the energy density of a ferromagnetic material for N randomly oriented exchange coupled grains is given as:

$$E_{total} = A\sum_{i=1}^{N}(\vec{\bigtriangledown}\phi)^2 + K_u sin^2\phi + \sum_{i=1}^{N} K_i sin^2(\phi - \phi_i) - \vec{H}\cdot\sum_{i=1}^{N}\vec{m}_i - \frac{1}{2}\vec{H}_{stray}\cdot\sum_{i=1}^{N}\vec{m}_i \tag{2}$$

where, ϕ_i and $\vec{m}_i$ are the directions of the local EA and the magnetization vector of the ith grain, respectively. Depending on the degree of misalignment of EA and exchange energy, the reversal mechanism varies. For example, if the randomness outweighs the exchange energy, then the rotational symmetry of the magnetization is broken leading to collapse of hard axis [8], formation of ripple domains [16] and non-trivial 360° domain walls [17].

In our previous work, it was shown that presence of dispersion in local grain anisotropy in single layer Co films affects the magnetization reversal, domain structure [7] and after-effect relaxation [18]. However, magnetization reversal in multilayers can be different compared to their thin film counterparts because in addition to local properties, reversal in the former also depends on inter-layer couplings. Depending on the nature of NM spacer, FM layers can experience different kinds of interactions. For metallic spacers, in addition to dipolar coupling the inter-layer interaction is attributed to Ruderman-Kittel-Kasuya–Yosida (RKKY) coupling mediated by conduction electrons [19, 20]. Similarly for insulating spacers the FM layers only experience dipolar coupling. In addition, presence of magnetic Dzyaloshinskii-Moriya interaction (DMI) in FM/NM/FM heterostructures may lead to interlayer coupling between the FM layers [21]. This may lead to three dimensional complex magnetic structures. E.g. Vedmedenko *et al.* [21] suggests that a competing interaction between DMI and RKKY can lead to intrinsic separation of columnar skyrmions which are future potential candidates for magnetic memory devices.

In our previous work, we investigated the magnetization reversal in the presence of uniaxial and random anisotropies in [$Co_{80}Fe_{20}$ (t_{CoFe})/ Al_2O_3 (t

=3 nm)]$_9$, multilayer systems where t_{CoFe} = 1.6 nm [22] and 1.8 nm [17], respectively. The uniaxial anisotropy in these samples were induced by applying a magnetic field during their deposition and the random anisotropy due to the granularity of thin films. In t_{CoFe} = 1.6 nm multilayers, the competing dipolar interactions along with Neel coupling gives rise to modulated incommensurate phases which is similar to axial next-nearest-neighbor Ising (ANNNI) type coupling. However, we reported that for t_{CoFe} = 1.8 nm multilayers, strong random anisotropy leads to the formation of 360° domain walls. In both these systems, the thickness of the spacer layer was kept constant. In this work we aim to investigate magnetization reversal in dipolarly coupled Co/AlO_X/Co trilayers having uniaxial and random anisotropies by varying the thickness of the insulating spacer layer (AlO_X). In contrast to ref [22] and [17] the uniaxial anisotropy in the present work was induced due to oblique angle deposition by sputtering [7, 18, 23, 24, 25, 26, 27, 28]. We report that even for large spacer thickness a layer-by-layer reversal is observed which is mainly controlled by the random anisotropy. Micromagnetic simulations using object oriented micromagnetic framework (OOMMF) software [29] were carried out considering both uniaxial and random anisotropies to explain the experimental results.

2. Experimental details:

We have studied Co/$AlO_X(t)$/Co trilayer samples with various thickness of AlO_X spacer layer. The thickness of both the Co layers (t_{Co}) was 10 nm for all the samples. Thin films were prepared by magnetron sputtering in a HV chamber manufactured by Mantis Deposition Ltd., UK. Due to the geometry of the system, the angle between the substrate normal and the incident flux from the target is 30°. In such oblique deposition condition, the grains grow in columnar form with a tilt towards the deposition angle, hence the shape anisotropy contributes in the effective uniaxial anisotropy of the film [7, 18, 27, 28]. Following samples were prepared on Si(100) substrates: (i) Single layer Co (Sample A) and (ii) bilayers of Co thin films where the thickness (t) of the spacer AlO_X layer was varied from 8 to 90 nm as shown schematically in supplementary Fig. S1. We have prepared a series of samples with spacer thicknesses of t = 8, 23, 33, 45, and 90 nm. For detailed discussion, here we have chosen two spacer thicknesses i.e. t = 8 and 90 nm to represent lower and higher spacer thickness regime, respectively. The sample names together with their structure have been summarized in Table 1. The bottom and top

Table 1: Details of sample names, their structure along with their spacer thickness.

Sample Name	**Sample structure on Si(100) substrate**
Sample A	AlO_X(3 nm)/Co(10 nm)/AlO_X(3 nm)
Sample B	AlO_X(3 nm)/Co(10 nm)/AlO_X(**8** nm)/Co(10 nm)/AlO_X(3 nm)
Sample C (for XTEM study)	AlO_X(3 nm)/Co(10 nm)/AlO_X(**23** nm)/Co(10 nm)/AlO_X(3 nm)
Sample D	AlO_X(3 nm)/Co(10 nm)/AlO_X(**90** nm)/Co(10 nm)/AlO_X(3 nm)

Co layers have been labelled as Co_1 and Co_2, respectively (supplementary Fig. S1). Sample A was prepared to compare the domains with those of samples B and D. The base pressure inside the sputtering chamber was better than 5×10^{-8} mbar. The deposition pressures for Co and AlO_X were 4×10^{-3} and 3×10^{-3} mbar, respectively. The Co and AlO_X layers were deposited using DC and RF sputtering at the rates of 0.022 nm/s and 0.007 nm/s respectively, at room temperature.

Structural characterization was performed using cross-sectional transmission electron microscopy (XTEM), time of flight secondary ion mass spectroscopy (TOF-SIMS5 of ION-TOF GmbH, Germany) and X-ray reflectivity (XRR). Electron transparent XTEM samples were prepared using mechanical thinning followed by low energy Ar^+ ion milling. The magnetization reversal was studied by magneto-optic Kerr effect (MOKE) based microscopy. Further, to know the magnetization depth profile, polarized neutron reflectivity (PNR) measurements were performed at TREFF and MARIA [30] reflectometers at FRM II at Munich, Germany. It should be noted that for both of these two neutron reflectometers the guiding field was about $\mu_0 H \sim$ -1 mT for keeping the neutron polarization. Further, to qualitatively understand the experimental observations, micromagnetic simulations were performed using object-oriented micromagnetic framework (OOMMF) software.

3. Results and discussion

Fig. 1 (a) shows the bright field (BF) cross-sectional transmission electron microscopy (XTEM) micrograph for sample C with its native SiO_2 on the Si (100) substrate. Fig. 1 (b) and (c) show the high-resolution XTEM images

of Co_1 and Co_2 layers, respectively, taken along the [011] zone axis of the Si substrate. These images reveal the polycrystalline nature of the Co layers. The thickness and the densities of the layers were determined from X-ray reflectivity (XRR) measurements (supplementary Fig. S2). The elemental depth profile and the quality of the layers were determined by using high resolution time of flight secondary ion mass spectroscopy (TOF-SIMS) for sample B as shown in Fig. 2, where the individual layers are clearly resolved in the $Co/AlO_X/Co$ matrix. The full width at half maxima for each layer intersected with each other indicating no interdiffusion. Since all the samples have been grown under similar conditions, it is therefore expected that the other samples also have a similar layer structure.

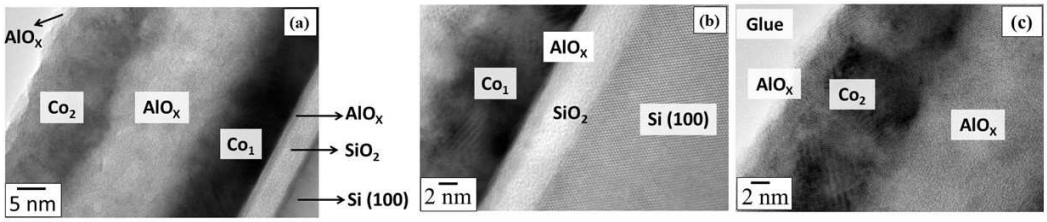

Figure 1: (a) Bright field (BF) cross-sectional transmission electron microscopy (XTEM) images of sample C. High resolution images of the cobalt layers (b) Co_1 and (c) Co_2 taken along the [011] zone axis of Si substrate.

Figure 3 shows the hysteresis loops and the corresponding domain images measured by longitudinal magneto-optic Kerr effect (LMOKE) based microscopy along EA for samples A, B and D, respectively. Figure 3(a) shows a single stepped hysteresis loop for sample A. As reported previous work [7], Co (10 nm) thin film prepared by oblique deposition showed uniaxial anisotropy with the presence of small random anisotropy. The rectangular shaped LMOKE hysteresis loop in Fig. 3 (a) indicates that magnetization reversal occurs via domain wall motion which is evident by the domain images shown in Fig. 3(b)–(e). The dark and grey contrasts correspond to positive and negative magnetized states. Field points corresponding to Fig. 3(b)–(e) are described in Fig. 3(a). It should be noted that sample A investigated in this paper and the results shown on a similar sample reported in ref. [7] have been prepared from two different Co targets. However, these samples exhibit similar anisotropy behaviour. Results from sample A have been shown in this paper to compare the magnetic properties of a single Co layer with those of

samples B and D having dipolarly coupled Co layers.

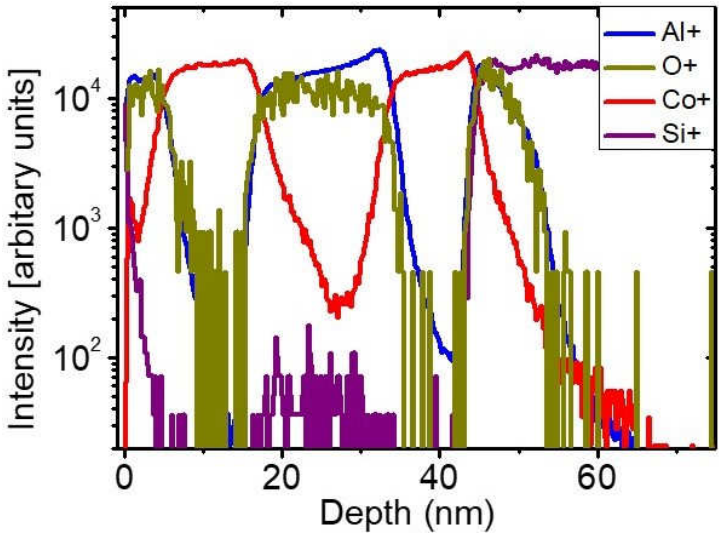

Figure 2: Elemental depth profile measured by SIMS for sample B i.e. Si (100)/AlO_X (3 nm)/Co (10 nm)/AlO_X (8 nm)/Co(10 nm)/AlO_X (3 nm).

A two stepped LMOKE hysteresis loop was observed for both samples B and D as shown in Fig. 3(f) and (l), respectively. The domain structures of sample B are shown in Fig. 3 (g)-–(k). At positive saturation, a single domain state with dark contrast (Fig. 3(g)) is observed. As the applied field is increased in the negative direction, the first magnetization reversal ($\mu_0 H = -3.7$ mT) is accompanied by large domains (Fig. 3(h)). It is also observed in Fig. 3(h) that some fine domains have nucleated in the region where reversal has already occurred. The field point (i) and the domain image in Fig. 3(i) corresponds to the sample state where one of the Co layers is completely reversed. By increasing the magnetic field, the second reversal ($\mu_0 H = -13.5$ mT) is accompanied by fine domains (Fig. 3(j)). Further increasing the field, the sample finally gets saturated to the positive state (Fig. 3(k)). The two reversal steps and corresponding different domains indicate the layer-by-layer reversal of the two Co layers which can be better visualized by the video SV1 as supplementary information. This video is the movie showing layer-by-layer magnetization reversal of sample B along one branch of hysteresis loop. Similar reversal behavior was observed also for the other branch of the hysteresis loop.

Further increasing the spacer thickness e.g. in sample D ($t = 90$ nm),

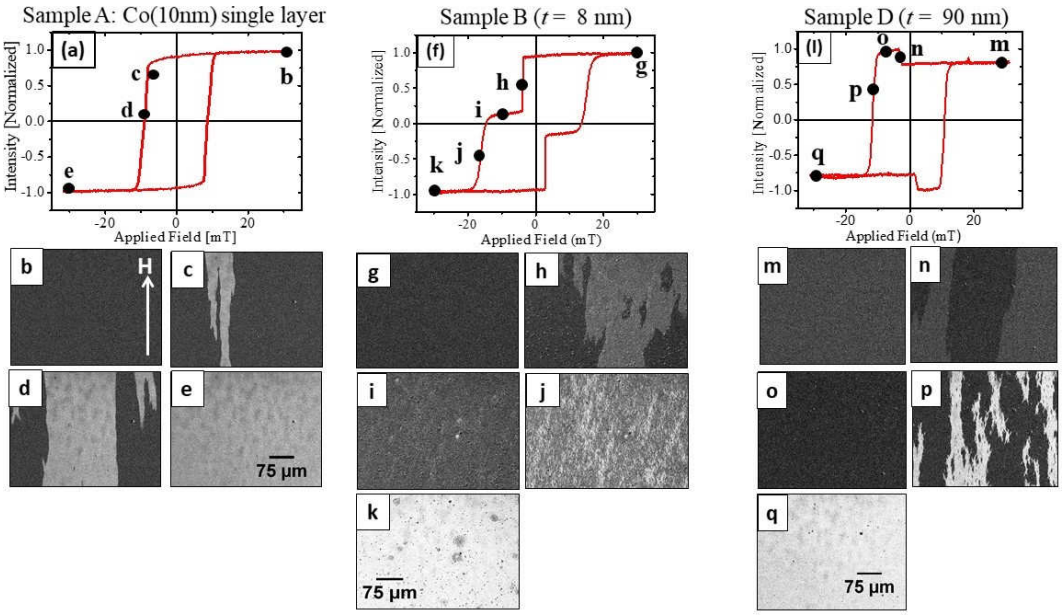

Figure 3: LMOKE hysteresis loops for samples A, B and D are shown in (a), (f) and (l), respectively. The domain images observed by Kerr microscopy for samples A, B and D are shown in (b)-–(e), (g)-–(k) and (m)–(q), respectively, and the corresponding field points are marked in their respective hysteresis loops.

we still observe a two stepped hysteresis loop implying a layer-by-layer reversal of the magnetization. The first and second reversal for this sample is accompanied by large stripe (Fig. 3(n)) and small branched domains (Fig. 3(p)), respectively. For better visualization supplementary video SV2 is provided showing magnetization reversal for one branch of hysteresis of sample D. Comparing Fig. 3 (j) and (p), it is observed that the domain images are different which indicates the effect of dipolar coupling because of increase in spacer thickness. A plateau-like feature in the hysteresis loop (Fig. 3(o)) may be due to the interference of the reflected light from the different layers [31]. This can occur due to different structural and magnetic properties of individual Co layers. However, we later show in OOMMF simulations that in the present case layer-by-layer reversal occurs due to the presence of random anisotropy in addition to growth induced uniaxial anisotropy.

Dipolar coupling is a major parameter which influences the reversal in such FM/NM/FM multilayers. Labrune *et al.* [32] have theoretically showed that for weakly coupled systems and in the absence of any exchange coupling,

each Co layer of the stack can individually respond to the change in the magnetic field. Hence, for decoupled Co layers, magnetization reversal behaviour will be similar to that of the corresponding single layer. In such decoupled multilayers, a single stepped hysteresis loop is expected in which the coercive and saturation fields are comparable for the magnetic single layer. Therefore, two stepped hysteresis loop in sample D (Fig. 3(k)) indicates that dipolar coupling is still non-vanishing even at spacer thickness of $t = 90$ nm.

By using MOKE microscopy, it is difficult to know the magnetization depth profile of the Co layers, therefore we have performed polarized neutron reflectivity (PNR) measurements in specular mode. PNR stands out as a unique technique because of its capability to resolve laterally averaged magnetization along the depth of the sample[33, 34]. The momentum transfer along the axis perpendicular to the sample surface i.e. Z-axis is given by:

$$q = q_z = \frac{4\pi sin\theta}{\lambda} \tag{3}$$

where, q_z = momentum transfer perpendicular to the surface, θ is the angle of incidence (equal to angle of reflection) and λ is the neutron wavelength. Since neutrons have a magnetic moment, they interact with the magnetization of the sample. Hence, the measurement of reflected intensity as a function of q_z provides the depth dependent information of magnetization in the thin film [33, 34]. Depending on the incident and final spin state of the neutron, four cross sections such as R^{++}, R^{--}, R^{+-}, and R^{-+} can be measured. The plus and minus signs indicate polarizations of the incident and reflected neutrons parallel or antiparallel to the applied external field, respectively. The R^{++} and R^{--} cross sections are called non-spin flip (NSF) and arise due to periodicities of the structure and magnetization components collinear to $\vec{H}$. The R^{+-} and R^{-+} reflectivities termed as spin flip (SF), channels. These are exclusively of magnetic origin and correspond to the in-plane magnetization components perpendicular (transverse magnetization) to $\vec{H}$. The PNR measurements were performed by positively saturating the sample and then reversing the field to a negative value. This means during the measurements the field was kept parallel to the guiding field. The fittings were performed using GenX [35] software which is based on Parratt′s formalism [36].

Fig. 4 shows the NSF data for sample B measured by PNR performed at the TREFF reflectometer. The experimental data is shown by open circles (red for R^{++} and blue for R^{--}) along with their fits (solid lines). It should be noted that the fitted curve considers the error bars, however the error

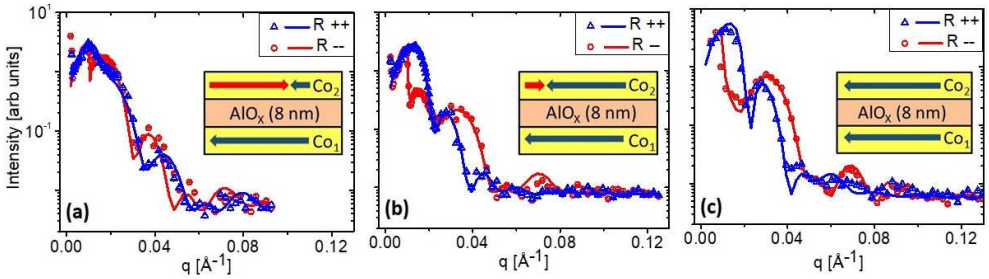

Figure 4: PNR data (open circles and open triangles) with error bars and fits (solid lines) for Sample B at (a) close to coercivity $\mu_0 H_c = -7$ mT, (b) $\mu_0 H = -18$ mT and (c) negative saturation ($\mu_0 H = -100$ mT). It should be noted that the error bars are very small. The inset in each graph shows the magnetization orientations of the two Co layers extracted from the fits. The bottom and top Co layers are labelled as Co_1 and Co_2, respectively, as described in sample's schematic (supplementary Fig. S1).

bars are very small. Near coercive field of $\mu_0 H \sim -7$ mT (Fig. 4(a)), for small values of q, $R^{++} \sim R^{--}$ indicating the demagnetized state of the sample. From the fits, it is found that the magnetization of the Co_1 has switched along the field whereas the Co_2 has partially reversed (20%) as shown in the inset of Fig. 4(a). PNR analysis complements the domain image shown for Sample B in Fig. 3(h). On increasing the field to $\mu_0 H = -18$ mT (Fig. 4(b)), it is observed that near the plateau of total reflection the $R^{--} > R^{++}$ implying that the sample is negatively magnetized. Analysis of the PNR data indicate the reversal of the Co_2 layer is along the field direction as shown in the inset of Fig. 4(b). The magnetization state in the Co layers analyzed from the PNR are complemented by Fig. 3(i). PNR data shown in Fig. 4 (c) was measured at negative saturation ($\mu_0 H = -100$ mT). The fits reveal that both the Co layers are negatively saturated as shown in the inset of Fig. 4(c). Hence, from Fig. 4 it is inferred that the Co layers are undergoing dipolar-coupled layer-by-layer magnetization reversal. The figure of merit for the fits shown in Fig. 4(a), (b) and (c) were 1.82×10^{-1}, 1.72×10^{-1} and 1.12×10^{-1}, respectively. On reversing the model, i.e. considering the magnetization reversal of Co_2 layer first followed by reversal of Co_1 layer, we were not able to fit the PNR data. Similar dipolar-coupled layer-by-layer magnetization reversal is observed in Sample D (see Fig. S3 and its corresponding description in the supplementary information). A small transverse component of magnetization has been observed (see Fig. S3).

The layer-by-layer reversal observed from LMOKE and PNR data observed can be due to different magnetizations of Co layers, interlayer competing effect, presence of random anisotropy ($K_{\rm r}$) etc.. Our previous reports have shown the presence of random anisoropy present in the Co single layer system (sample A) [7]. Hence, in addition to uniaxial aniostropy, we expect the presence of ($K_{\rm r}$) in these samples. Using OOMMF simulations, our previous report shows that presence of high random anisotropy in a uniaxial system leads to formation of 360° domain walls [17]. Hence, it is expected that the presence of small random anisotropy will have some effect, particularly on magnetization reversal. Therefore, in order to understand the magnetization reversal observed in the experiments, OOMMF[29] simulations were carried out such that a small random anisotropy ($K_{\rm r}$) was incorporated in addition to the uniaxial anisotropy ($K_{\rm u}$).

In OOMMF simulations, we considered different spacer layers (t) = 8, and 90 nm separating two Co (10 nm) layers. For further discussion, the samples studied for simulations are labelled as sample SS1 and SS2 for the spacer layer thickness (t) = 8, and 90 nm, and hence corresponds to samples B and D, respectively. The lateral size of the sample was taken to be 304 x 304 nm^2. The cell size and the saturation magnetization were considered to be 3.2 x 3.2 x 2 nm^3 and 1.44 x 10^6 A/m, respectively [22]. Here random anisotropy was taken in order to mimic the randomness around the direction of the uniaxial anisotropy keeping its magnitude constant. This was to account for the variation in local anisotropy due to the misalignment of grains which was observed experimentally in the real thin films. In the simulations the uniaxial ($K_{\rm u}$) and random ($K_{\rm r}$) anisotropy values were chosen to be 0.18×10^6 J/m^3 and 0.05×10^6 J/m^3, respectively.

Figure 5 shows OOMMF simulated longitudinal hysteresis loops (x- component of magnetization i.e. $m_{\rm X}$) along with the domain images for samples SS1, and SS2. Simulations were performed by negatively saturating the sample and then reversing the field to positive direction. This protocol was followed in order to reproduce the experimental finding from the Kerr microscopy and PNR experiments. The subscripts in any domain image number of Fig. 5 is to be read as: 1 for bottom (e.g. b_1) and 2 for top Co layer (e.g. b_2), respectively. Two stepped OOMMF simulated longitudinal hysteresis loops (Fig. 5 (a)) for 8 nm spacer thickness (i.e. sample SS1) are observed. The shapes of the simulated loops are similar to the experimentally observed MOKE loops (Fig. 3 (f)). The reversal is better understood from the domain images shown in Fig. 5. In the images the red and blue pixel implies $m_{\rm X} < 0$

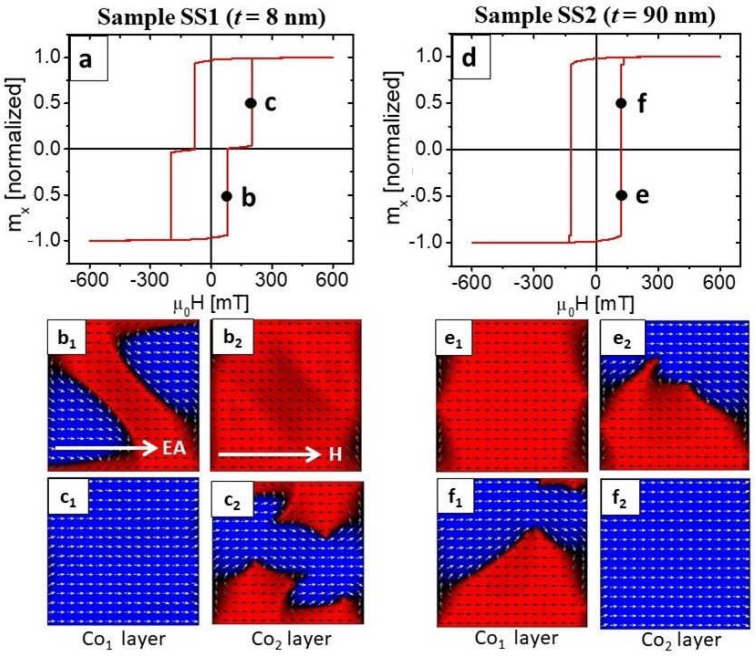

Figure 5: OOMMF simulated hysteresis along with domain images for samples SS1, and SS2 with $K_u = 0.18 \times 10^6$ J/m^3, $K_r = 0.05 \times 10^6$ J/m^3. The red and blue pixels correspond to magnetization $m_X < 0$ and $m_X > 0$, respectively. The suffix '1' and '2' after the domain image number (e.g. b_1, b_2, c_1, c_2 etc.) refers to the Co_1 and Co_2 layers, respectively.

and $m_X > 0$, respectively. By reversing the field towards positive direction, at field point 'b' for sample SS1 (Fig. 5(a)), reverse domains are observed for the Co_1 layer (Fig. 5(b1)). On increasing the field to point 'c' (Fig. 5(a)), it is observed that Co_1 reversed completely (Fig. 5(c1)), whereas the Co_2 layer is partially magnetized (Fig. 5(c2)). On increasing the field further, Co_2 gets saturated and the sample reaches a positive single domain state. Similar results were obtained for periodic boundary conditions and keeping all the parameters same as above. Hence, the OOMMF simulations revealed layer-by-layer magnetization reversal in sample SS1 which has strong inter-layer coupling.

These results are consistent with the experimental observations of the Kerr microscopy and PNR data revealing layer-by-layer magnetization reversal of the Co layers. The PNR data in Fig. 4 and supplementary information Fig. S3 revealed the antiparallel alignment of the two Co layers for both samples B and D, respectively. However, the OOMMF simulated hysteresis loop

is a single stepped loop for sample SS2 (Fig. 5(d)). The difference may be due to some additional bi-quadratic coupling in real sample arising because of roughness, which has not been incorporated in the present investigation. This is planned in future studies. It is noted that these simulations show different domain structures for sample SS2 as compared to sample SS1 indicating that dipolar coupling strongly governs the domain structure. Hence, the simulation results support the experimental findings observed by Kerr microscope. Further, the longitudinal hysteresis loop for sample SS2 is similar to the OOMMF hysteresis of Co (10 nm) single layer (SS3) (shown in supplementary Fig. S4 (a)). It indicates that both the Co layers are decoupled and reverse independently of applying the magnetic field. Therefore, the domain structure for these decoupled Co layers (sample SS2) were similar to that of sample SS3 shown in supplementary Fig. S4 (c-f). However, our experiments reveal that, the Co layers are not completely decoupled for sample D and the reversal is not similar to the simulated hysteresis. The experiment and simulations do not match well due to the values of various parameters used in OOMMF which may be different than those in the real thin films. It is worth mentioning that in the simulations considering only dipolar coupling it was not possible to observe the layer-by-layer magnetization reversal as shown in the supplementary Fig. S5. Hence, presence of non-negligible random anisotropy is a crucial ingredient for the layer-by-layer magnetization reversal in such magnetic multilayers.

4. Conclusion

We have shown the combined effect of dipolar coupling and random anisotropy on the magnetization reversal of ferromagnetic layers separated by an insulating spacer. Dipolar-coupled layer-by-layer magnetization reversal of the Co layers was evidenced by Kerr microscope and PNR measurements. The experimental results were supported by OOMMF simulations in which uniaxial and random anisotropies were incorporated along with the dipolar coupling to elucidate layer-by-layer magnetization reversal in $Co/AlO_X/Co$ trilayers. Our studies show that the local dispersion in anisotropy can lead to an effective random anisotropy. The latter has significance depending on its strength compared to the other intrinsic anisotropy e.g. uniaxial one. Other parameters such as inter-layer coupling (dipolar and/or bi-quadratic) may have significant effects in the magnetization reversal. In a future work the effects of these parameters may be addressed. Although we studied the

FM/NM/FM trilayers for an insulating AlO_X, however, in principle our study can be extended to systems with metallic NM spacers (e.g. GMR structures). One should consider such random anisotropy in the formation of skyrmions in coupled layers or synthetic antiferromagnets.[5, 6, 21]

References

[1] C. Chappert, P. Bruno, B. Bartenlian, P. Beauvillian, A. Bounouh, R. Megy, P. Veillet, Magnetic anisotropy and interlayer exchange coupling in Fe (110)/Au (111) ultrathin films, J. Magn. Magn. Mater. 148 (1-2) (1995) 165–166.

[2] S. Parkin, X. Jiang, C. Kaiser, A. Panchula, K. Roche, M. Samant, Magnetically engineered spintronic sensors and memory, Proc. IEEE 91 (5) (2003) 661–680.

[3] P. Grünberg, R. Schreiber, Y. Pang, M. Brodsky, H. Sowers, Layered magnetic structures: Evidence for antiferromagnetic coupling of Fe layers across Cr interlayers, Phys. Rev. Lett. 57 (19) (1986) 2442.

[4] S. S. Parkin, C. Kaiser, A. Panchula, P. M. Rice, B. Hughes, M. Samant, S.-H. Yang, Giant tunnelling magnetoresistance at room temperature with MgO (100) tunnel barriers, Nat. Mater. 3 (12) (2004) 862.

[5] J. Chatterjee, S. Auffret, R. Sousa, P. Coelho, I.-L. Prejbeanu, B. Dieny, Novel multifunctional RKKY coupling layer for ultrathin perpendicular synthetic antiferromagnet, Sci Rep. 8 (1) (2018) 11724.

[6] S. Kang, N. Kim, H. Kwon, J. Choi, B. Min, C. Won, The spin structures of interlayer coupled magnetic films with opposite chirality, Sci Rep. 8 (1) (2018) 2361.

[7] N. Chowdhury, S. Bedanta, Controlling the anisotropy and domain structure with oblique deposition and substrate rotation, AIP Adv. 4 (2) (2014) 027104.

[8] O. Idigoras, A. Suszka, P. Vavassori, P. Landeros, J. Porro, A. Berger, Collapse of hard-axis behavior in uniaxial Co films, Phys. Rev. B 84 (13) (2011) 132403.

[9] E. Chudnovsky, W. Saslow, R. Serota, Ordering in ferromagnets with random anisotropy, Phys. Rev. B 33 (1) (1986) 251.

[10] R. Coehoorn, D. De Mooij, J. Duchateau, K. Buschow, Novel permanent magnetic materials made by rapid quenching, J. Phys. Colloques 49 (C8) (1988) C8–669.

[11] R. Skomski, Micromagnetic localization, J. Appl. Phys. 83 (11) (1998) 6503–6505.

[12] J. Liu, C. Luo, Y. Liu, D. Sellmyer, High energy products in rapidly annealed nanoscale Fe/Pt multilayers, Appl. Phys. Lett. 72 (4) (1998) 483–485.

[13] D. Jiles, Introduction to magnetism and magnetic materials, CRC press, (2015).

[14] R. Alben, J. Becker, M. Chi, Random anisotropy in amorphous ferromagnets, J. Appl. Phys. 49 (3) (1978) 1653–1658.

[15] G. Herzer, Grain size dependence of coercivity and permeability in nanocrystalline ferromagnets, IEEE Trans. Magn. 26 (5) (1990) 1397–1402.

[16] D. Smith, K. Harte, Noncoherent switching in permalloy films, J. Appl. Phys. 33 (4) (1962) 1399–1413.

[17] N. Chowdhury, W. Kleemann, O. Petracic, F. Kronast, A. Doran, A. Scholl, S. Cardoso, P. Freitas, S. Bedanta, 360° domain walls in magnetic thin films with uniaxial and random anisotropy, Phys. Rev. B 98 (13) (2018) 134440.

[18] N. Chowdhury, S. Mallick, S. Mallik, S. Bedanta, Study of magnetization relaxation in Co thin films prepared by substrate rotation, Thin Solid Films 616 (2016) 328–334.

[19] P. Bruno, C. Chappert, Oscillatory coupling between ferromagnetic layers separated by a nonmagnetic metal spacer, Phys. Rev. Lett. 67 (12) (1991) 1602.

[20] P. Bruno, C. Chappert, Ruderman-Kittel theory of oscillatory interlayer exchange coupling, Phys. Rev. B 46 (1) (1992) 261.

[21] E. Y. Vedmedenko, P. Riego, J. A. Arregi, A. Berger, Interlayer dzyaloshinskii-moriya interactions, Phys. Rev. Lett. 122 (25) (2019) 257202.

[22] S. Bedanta, E. Kentzinger, O. Petracic, W. Kleemann, U. Rücker, T. Brückel, A. Paul, S. Cardoso, P. Freitas, Modulated magnetization depth profile in dipolarly coupled magnetic multilayers, Phys. Rev. B 74 (5) (2006) 054426.

[23] D. Smith, M. Cohen, G. P. Weiss, Oblique-incidence anisotropy in evaporated permalloy films, J. Appl. Phys. 31 (10) (1960) 1755–1762.

[24] Y. Fukuma, Z. Lu, H. Fujiwara, G. Mankey, W. Butler, S. Matsunuma, Strong uniaxial magnetic anisotropy in CoFe films on obliquely sputtered Ru underlayer, J. Appl. Phys. 106 (2009) 076101.

[25] Y.-P. Fang, W. He, H.-L. Liu, Q.-F. Zhan, H.-F. Du, Q. Wu, H.-T. Yang, X.-Q. Zhang, Z.-H. Cheng, Surface morphology and magnetic anisotropy of obliquely deposited Co/Si (111) films, Appl. Phys. Lett. 97 (2) (2010) 022507.

[26] Paritosh, D. Srolovitz, Shadowing effects on the microstructure of obliquely deposited films, J. Appl. Phys. 91 (4) (2002) 1963–1972.

[27] S. Mallik, N. Chowdhury, S. Bedanta, Interplay of uniaxial and cubic anisotropy in epitaxial Fe thin films on MgO (001) substrate, AIP Adv. 4 (9) (2014) 097118.

[28] S. Mallick, S. Mallik, B. B. Singh, N. Chowdhury, R. Gieniusz, A. Maziewski, S. Bedanta, Tuning the anisotropy and domain structure of Co films by variable growth conditions and seed layers, J. Phys. D 51 (27) (2018) 275003.

[29] M. J. Donahue and D. G. Porter, OOMMF User's Guide, version 1.0, Tech. rep. NIST Report 6376 (1999)

[30] S. Mattauch, A. Koutsioubas, S. Pütter, Maria: Magnetic reflectometer with high incident angle, Journal of large-scale research facilities JLSRF 1 (2015) 8.

[31] S. Zhang, J. Gao, W. Xia, L. Chen, Y. Tang, D. Li, S. Tang, Y. Du, Enhancement of longitudinal magneto-optical Kerr effect in HfO2/Co/HfO2/Al/Silicon thin films, Opt Commun. 321 (2014) 226–229.

[32] M. Labrune, H. Niedoba, Dipolar coupling effect in magnetic bilayer system, Eur. Phys. J. B 27 (1) (2002) 103–109.

[33] S. Sinha, E. Sirota, Garoff, S, H. Stanley, X-ray and neutron scattering from rough surfaces, Phys. Rev. B 38 (4) (1988) 2297.

[34] H. Zabel, X-ray and neutron reflectivity analysis of thin films and superlattices, Appl. Phys. A 58 (3) (1994) 159–168.

[35] http://genx.sourceforge.net.

[36] L. G. Parratt, Surface studies of solids by total reflection of X-rays, Phys. Rev. s95 (2) (1954) 359.

Acknowledgement

We thank National Institute for Science Education and Research (NISER) and the Department of Atomic Energy of the Government of India for the financial support. Financial support from DST-DAAD (DST Sanction Letter No: INT/FRG/DAAD/P-219/2012) to carry out the PNR measurements is greatly acknowledged. We thank Prof. P. V. Satyam for extending help for the XTEM measurements. We thank Miss Srijani Mallik, Mr. Sovakara Singh and Mr. Swapna Sindhu Mishra for valuable discussions. We also thank Dr. J. V. Yeldho for proof reading of the manuscript.